Mechanical properties of monolayer sulphides : a comparative study between MoS_2, HfS_2 and TiS_3

Mechanical Properties of Monolayer Sulfides of TiS_3, HfS_2 and MoS_2

Jun Kang,[1, *] H. Sahin,[1, †] and F. M. Peeters[1]

[1]*Department of Physics, University of Antwerp, Groenenborgerlaan 171, B-2020 Antwerpen, Belgium*

(Dated: February 3, 2015)

In this study, motivated by the recent synthesis of hexagonal monolayers of Aluminum Nitride, we study it's number of layer dependent electronic and optical properties. We also found that optical properties that is different for monolayer, fewlayer and bulk can utilized as an efficient way for the determination of the morphology of the synthesized materials. In this study, motivated by the recent synthesis of hexagonal monolayers of Aluminum Nitride, we study it's number of layer dependent electronic and optical properties. We also found that optical properties that is different for monolayer, fewlayer and bulk can utilized as an efficient way for the determination of the morphology of the synthesized materials. In this study, motivated by the recent synthesis of hexagonal monolayers of Aluminum Nitride, we study it's number of layer dependent electronic and optical properties. We also found that optical properties that is different for monolayer, fewlayer and bulk can utilized as an efficient way for the determination of the morphology of the synthesized materials. In this study, motivated by the recent synthesis of hexagonal monolayers of Aluminum Nitride, we study it's number of layer dependent electronic and optical properties. We also found that optical properties that is different for monolayer, fewlayer and bulk can utilized as an efficient way for the determination of the morphology of the synthesized materials.

PACS numbers:

I. INTRODUCTION

The high mechanical strength and electronic quality of transition metal sulphides (TMSs) have attracted understanding the chemistry and physics of these materials.[1–4] Most of the TMSs form layered compounds where closely-packed layers are held together by weak van der Waals forces. However, Ultra-thin TMSs have recently emerged as promising materials for new nanoscale devices in a wide variety of applications.[5,6] In these device applications, especially the semiconducting nature of ultra-thin sulphides make them superior to graphene, which is a semimetal. Chemical versatility of ultra-thin TMSs is another reason of growing interest on these materials.[7]

The first synthesized member of ultra-thin TMSs is MoS_2. By using micromechanical cleavage method, succesful synthesis of sinlge layer MoS_2 was achieved by Novoselov et al.[8] Shortly after this study, optical spectroscopy measurements on number of layer dependent properties of MoS_2 revealed that effect of quantum confinement leads to a crossover to a direct-gap material in the limit of the single monolayer.[9] Significant enhancement in luminescence quantum efficiency of single layer structure attracted further interest on this materal class. Furthermore the experiments on the stiffness and breaking strength of monolayer MoS_2 showed that its mechanical strength is comparable to that of steel.[10] These findings on MoS_2 triggered the efforts on using TMSs for flexible electronic nanodevice applications.

Following MoS_2, several new elements of TMSs emerged such as WS_2, VS_2, HfS_2 and TiS_3. It was shown by several groups that suphides of Mo and W have quite similar properties such as lattice parameter and electronic structure[11–13] Although there were some findings on the high moisture responsiveness of ultrathin VS_2,[14] the literature on the evidence of single layers of this material is sparse. In addition, dimensionality dependent electronic properties of HfS_2, from bulk to single layer, was reported.[15] Differing from single layers of MoS_2, WS_2 and VS_2 which are in 1H phase where the metal atom have trigonal prismatic coordination, single layer HfS_2 forms a octahedral phase (1T) in its ground state. In addition to these, recent experiments reported the successful synthesis of single layer TiS_3 which has a entirely different crystal symmetry.[16] It was shown that TiS_3 layers which are isolated by viscoelastic mechanical exfoliation have quite high photoresponsivity and therefore they are promising materials for nanoscale transistors and optoelectronic devices.

In this work we investigate the mechanical performance of single layer TMSs TiS_3, HfS_2 and MoS_2. Although the mechanical response of MoS_2 well-studied by experimental and theoretical groups in past few years, recently emerged structures TiS_3 and HfS_2 have not been investigated before. While our calculations on MoS_2 allow us to examine the reliability of the computational methodology, calculations on TiS_3 and HfS_2 reveal the mechanical characteristics of these novel structures.

The paper is organized as follows. Our computational details are given in Sec. II. Ground state structural and electronic properties of TiS_3, HfS_2 and MoS_2 outlined in Sec. III. We also calculate vibrational properties of these structures in Sec III. Our results on elastic parameters, ultimate strength and strain dependent electronic structure are presented in Sec.IV. We discuss our results in SecV.

II. COMPUTATIONAL METHODOLOGY

The calculations are performed using the frozen-core projector augmented wave method[25] as implemented in the Vienna *ab initio* simulation package (VASP).[23,24] The generalized gradient approximation of Perdew-Burke-Ernzerhof (GGA-PBE)[26] is chosen as exchange-correlation functional. Energy cutoff for plane-wave expansion is set to 400 eV. Brillouin zone sampling is performed with Monkhorst-Pack (MP) special k-point meshes[27] including the Γ-point. For MoS_2 and HfS_2 a grid of 12×12×1 is used, and for TiS_3 a grid of 7×11×1 is used. A vacuum layer larger than 10 Å is added to avoid interaction between adjacent images. All atoms are allowed to relax until the calculated Hellmann-Feynman force on each atom is smaller than 0.01 eV/Å.

III. GROUND STATE PROPERTIES OF TIS_3, HFS_2 AND MOS_2

A. Atomic Structure

1. paragraph MoS2
2. paragraph TiS3
3. paragraph HfS2

B. Vibrational Spectrum

1. paragraph MoS2
2. paragraph TiS3
3. paragraph HfS2

C. Electronic and Magnetic Properties

1. paragraph MoS2
2. paragraph TiS3
3. paragraph HfS2

IV. MECHANICAL RESPONSE OF TIS_3, HFS_2 AND MOS_2

A. Elastic parameters

In-plane stiffness and Poisson's ratio are two important elastic parameters for 2D materials. The in-plane stiffness C is defined as $C = (1/S_0)(\partial^2 E_s/\partial\varepsilon^2)$, where S_0 is the equilibrium area of the 2D material, E_s is the strain energy (the energy difference between equilibrium and strained structures) and ε is the applied strain. A material with smaller C can be stretched more easily. The other parameter, Poisson's ratio ν, is the ratio of the transverse strain to the axial strain, namely, $\nu = -\varepsilon_{\text{trans}}/\varepsilon_{\text{axial}}$. C and ν can be obtained through calculating the strain-energy relationship, as described in Ref.17. First, we construct rectangular unit cells of MoS_2, TiS_3 and HfS_2, as shown in Fig. 1. The two lattice vectors are along x and y directions, respectively. For hexagonal MoS_2 and HfS_2, x and y correspond to the armchair and zigzag directions. By changing the lattice constants, we apply strains ranging from -0.02 to 0.02 along each directions, with a step of 0.01. Thus a data grid with 25 points is obtained. At each point we relax the internal atomic position, and calculate the strain energy E_s. The strain energy can be fitted by the formula $E_s = c_1{\varepsilon_x}^2 + c_2{\varepsilon_y}^2 + c_3\varepsilon_x\varepsilon_y$, in which ε_z and ε_a are the strain along x and y directions, respectively. The in-plane stiffness along x and y directions can be then calculated as $C_x = (1/S_0)(2c_1 - {c_3}^2/2c_2)$ and $C_y = (1/S_0)(2c_2 - {c_3}^2/2c_1)$. The Poisson's ratio along x and y directions can be obtained by $\nu_x = c_3/2c_2$ and $\nu_y = c_3/2c_1$. For structures with hexagonal symmetry, c_1 equals to c_2 in the harmonic region. Therefore, along x and y directions, the in-plane stiffness and Poisson's ratio of MoS_2 and HfS_2 are the same. On the other hand, TiS_3 exhibits anisotropic C and ν.

The calculated in-plane stiffness of MoS_2 is 124.24 N/m, which is in agreement with other DFT work.[13] A recent experiment reported a in-plane stiffness of 180±60 N/m,[18] which is also consist with our results. The effective Young's Modulus can be deduced from C/h by assuming a proper thickness h of the monolayer. Taking h=6.145 Å, which is the interlayer spacing in bulk MoS_2, the Young's Modulus of monolayer can be determined as 202.18 GPa. The Poisson's ratio of MoS_2 is calculated to be 0.25.

For TiS_3, C_x and C_y are different. We found C_x=83.33 N/m and C_y=133.56 N/m, in agreement with other calculations.[19] According to Ref.20. , the interlayer spacing in bulk TiS_3 is 8.706 Å. So the effective Young's Module are 95.72 GPa and 153.41 GPa along x and y, respectively. The Poisson's ratios are ν_x=0.11 and ν_y=0.18.

The in-plane stiffness of HfS_2 is found to be 79.86 N/m. Assuming a effective thickness as its bulk interlayer spacing 5.837 Å, the Young's Modulus is 136.82 GPa. The calculated Poisson's ratio is 0.19.

The calculated in-plane stiffness follows the trend $TiS_3(y)$ >MoS_2 >$TiS_3(x)$ >HfS_2. This trend can be understood in view of bond length and bond density in different materials. A smaller bond length (thus a stronger bond) and a higher bond density per unit area would lead to a larger in-plane stiffness. In MoS_2 and HfS_2, the metal-sulfur bond length is 2.41 Å and 2.55 Å, respectively. In TiS_3, there are three different types of bonds. Along the y direction there are two types, with bond length of 2.46 and 2.50 Å. The third type is along x direction, with bond length of 2.67 Å. The order of bond length is $TiS_3(x)$ >HfS_2 >$TiS_3(y)$ >MoS_2. Hence the in-

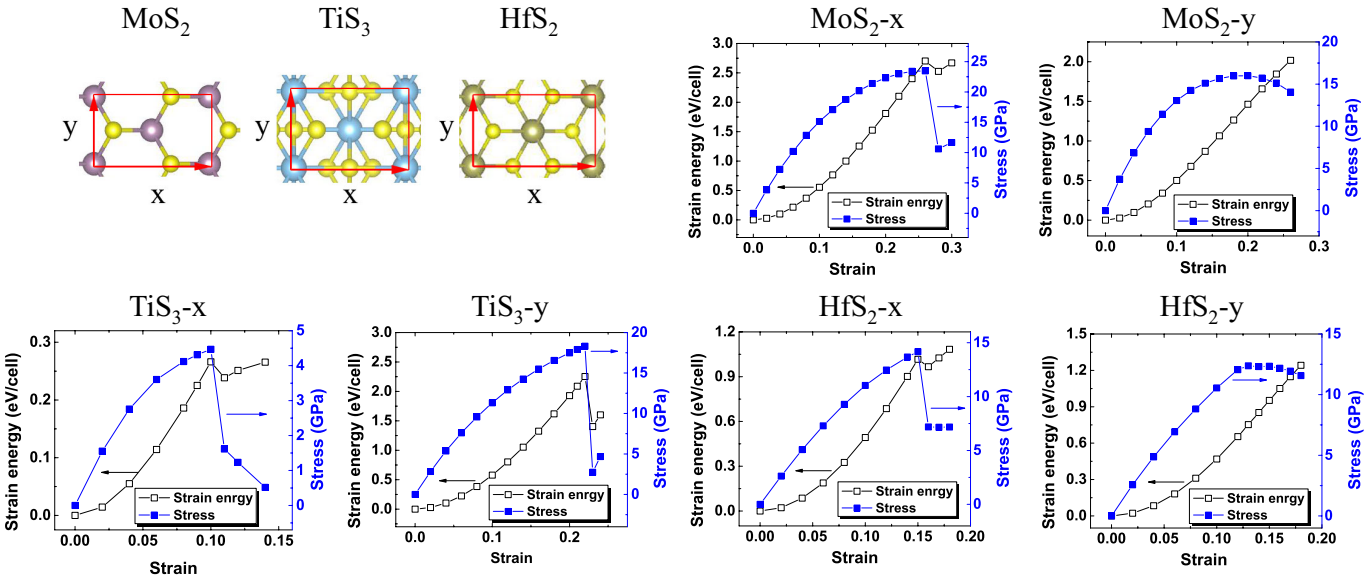

FIG. 1: The variation of strain energy and stress with uniaxial strain along x and y for MoS_2, TiS_3 and HfS_2. The rectangle unit cells used are also given.

plane stiffness of MoS_2 and $TiS_3(y)$ is larger than that of $TiS_3(x)$ and HfS_2, due to stronger bonds. On the other hand, in TiS_3, each Ti is eight-fold coordinated, whereas the metal atoms are six-fold coordinated in the other two materials. In addition, the density of Ti per unit area is larger than that of Mo and Hf. As a result, the bond density in TiS_3 is higher than those of MoS_2 and HfS_2. When bond strength is comparable, TiS_3 would have larger in-plane stiffness because of higher bond density. Thus the in-plane stiffness of $TiS_3(y)$ ($TiS_3(x)$) is larger than that of MoS_2 (HfS_2).

B. Ultimate strength

In this part we discuss the strain-stress relations of MoS_2, TiS_3 and HfS_2. We employ rectangular unit cells as shown in Fig. 1. Uniaxial strain is applied along x or y direction, and the cell vector perpendicular to the strain, as well as the atoms, is fully relaxed. In many cases, nano-structure materials undergo reconstructions when applied strain is large enough. To explore possible reconstructions, in our calculations we break the symmetry limitation of the monolayers before structure relaxation by randomly displacing a specified atom from its high symmetric position a little. If there is no reconstruction, the atom will go back after relaxation, and the original symmetry can be preserved. Using the effective thickness of the monolayers mentioned above, the stress along the strain direction can be obtained after structure optimization. With increasing strain, the stress will increase first, and then reach a maximum value at a critical strain value, which corresponds to the ultimate strength of the monolayer. When the strain exceeds the critical value, the structure become unstable. In Fig. 1 the stress and strain energy of MoS_2, TiS_3 and HfS_2 at different strain along x and y are presented.

With strain the symmetry of MoS_2 is lowered from D_{3h} to C_{2v}, therefore the mechanic response of MoS_2 become anisotropic under higher strain value. When strain is along x, the maximum stress of 23.48 GPa is achieved at ε_x=0.26. This is in good agreement with the 27.35 GPa at ε_x=0.28 in Ref.21 and the 24 GPa at ε_x=0.256 in Ref.22. It is also notable that when ε_x exceeds 0.26, there is a drop in the stress and strain energy, indicating a structure reconstruction of the monolayer. Indeed we find the C_{2v} symmetry is no longer preserved when ε_x exceeds 0.26. The structure deformation is non-reversible in this region even when the applied strain is removed. This is not observed in previous studies,[21,22] which probably results from the limitation of symmetry when doing structure relaxation in those works. With strain along y, the ultimate strength of MoS_2 is found to be 15.99 GPa at ε_y=0.20, agrees with the the 16.9 GPa at ε_y=0.19 in Ref.21 and the 15.6 GPa at ε_y=0.18 in Ref.22. We observe no reconstructions up to ε_y=0.26. The ultimate strength along the x and y directions shows obvious different. The anisotropy can be measured by a factor $\phi = \sigma_x/\sigma_y$, where σ_x and σ_y are the ultimate strength along x and y directions, respectively. The ϕ for MoS_2 is 1.47.

In TiS_3 monolayer, for strain along x, the ultimate strength is 4.45 GPa, with a ultimate strain of 0.10. When strain is along y, the ultimate strength and strain are 18.32 GPa and 0.22, respectively. In both cases, when the strain goes further than the ultimate strains, the monolayer undergoes non-reversible structure reconstructions which break the original C_{2h} symmetry, as indicated by a sudden reduce in strain energy and stress. The ultimate strength along x is much smaller than that

along y, with a anisotropy factor of 0.24. This can be attributed to the anisotropy in the structure of TiS_3. As mentioned above, the bond length of TiS_3 along x direction is much larger compared with the y direction. Therefore, the bond along x is weaker and easier to be break, leading to the small ultimate strength and strain.

For HfS_2, the ultimate strength and strain along x are 14.16 GPa and 0.15, respectively. Along y direction, these values are 12.38 GPa and 0.13. The anisotropy factor of ultimate strength is 1.14. Compared with 1-H MoS_2, the anisotropy in 1-T HfS_2 is smaller. Similar to TiS_3, reconstructions happen beyond the ultimate strain, breaking the C_{2h} symmetry. The reconstructions with strain along x is non-reversible, proved by a decrease in strain energy. However, when strain is along y, we find the deformation is minor between the reconstructed and unreconstructed structures. Therefore, the strain energy continue to grow when strain is larger than 0.13, suggesting a reversible reconstruction. Once the strain is released, the monolayer may return to the structure at $\varepsilon = 0$.

C. Band gap response under strain

Finally we investigate the response of band structure with the applied strain. We focus on the strain range in which no reconstruction happens. For MoS_2 and HfS_2, we use the primitive unit cell to calculate the band structure instead of the rectangle unit cell. The variation of band gap and the band structure of the monolayers with uniaxial strain, are illustrated in Fig 2. For MoS_2, the band gap monotonously decreases when the strain increases, in consistent with previous study. When strain is less than 0.1, the effects of x-strain and y-strain on the band gap are almost the same. Beyond this value, the gap decreasing in y-strain case is slightly faster than in x-strain case. When strain along x becomes larger than 0.2, the gap saturates to 0.45 eV. Moreover, strain modifies the band edge position of MoS_2. Without strain MoS_2 has a direct band gap at the K(L) point. When strain is applied, the band gap becomes indirect. The CBM state is located on the L-M$'$ path for strain along x, and on the K-Γ path for strain along y. Under small strain, the CBM is close to L or K. As the strain increases, the CBM moves towards M$'$ or Γ. The VBM transfers to the Γ point with strain along both x and y.

Compared with MoS_2, the band response to strain in TiS_3 is very different. In the strained structures, the CBM and VBM states remain at the Γ point. Furthermore, it shows strong anisotropy, as seen in Fig. 2. With increasing x-strain, overall the band gap shows a decreasing trend, and the magnitude is not large. From $\varepsilon_x = 0$ to $\varepsilon_x = 0.1$, the band gap reduction is about 0.1 eV. In case of y-strain, as the strain increases, the band gap becomes larger at first, and reaches 0.81 eV at $\varepsilon_y = 0.12$. When the strain further increases, the band gap become smaller. To explore the origin of such a non-monotonously behavior, we look into the orbital character of the CBM and VBM states. We find the CBM state of TiS_3 is from the d_{z^2} orbitals of Ti atoms, and this character doesn't change with strain. The effect of strain on CBM energy is also found to be small. However, the situation of VBM is different. When ε_y is smaller than 0.12, the VBM state consists of the d_{xz} orbitals of Ti atoms and p_x orbitals of the four-fold coordinated S atoms. Whereas when ε_y is larger than 0.12, the dominated orbitals of VBM state are the d_{xz} orbitals of Ti atoms and p_x orbitals of the two-fold coordinated S atoms. Due to the different orbital character, the response of VBM state to strain is different in these two cases. For $\varepsilon_y < 0.12$, the VBM energy decreases as strain increases. When $\varepsilon_y > 0.12$, the VBM energy increases with increasing strain. Therefore, the band gap increases at first, and then decreases.

In the case of HfS_2, without strain the monolayer is a indirect gap semiconductor with CBM at M (M$'$) and VBM at Γ. When x-strain is smaller than 0.1, the CBM is at M$\prime$ and the VMB is at Γ. The gap value slightly increases with increasing strain, as shown in Fig. 2. When x-strain is larger than 0.1, the CBM moves to the Γ point, while the VBM is still at Γ, leading to a indirect-direct gap transition. Because of the change of CBM character, the band gap now decreases with increasing x-strain. In the y-strain case, the VBM is also found at the Γ point in the whole range considered. When ε_y is smaller than 0.08, the CBM is at M. At ε_y=0.1, the CBM changes to the M$'$ point. At ε_y=0.12, the CBM is located at the Γ point, and indirect-direct gap transition happens. The variation of gap value with $\varepsilon_y < 0.1$ is very similar to that in the x-strain case. It is slightly larger with larger strain. From ε_y=0.1 to 0.12, the gap decreases a little. The origin is again the change of CBM, as in the x-strain case. Overall, the anisotropy of band gap variation with strain in HfS_2 is also small, especially in the small-strain range, similar to the case of MoS_2. In addition, the strain-induced indirect to direct gap transition may lead to possible applications of HfS_2 in optoelectronics.

V. ACKNOWLEDGEMENT

* Electronic address: jun.kang@uantwerpen.be
† Electronic address: hasan.sahin@uantwerpen.be

[1] F. Hulliger Crystal chemistry of the chalcogenides and pnictides of the transition elements
[2] D. W. Bruce, Transition Metal Sulphides: Chemistry and Catalysis, T. Weber, R. Prins and R. A. van Santen (eds),

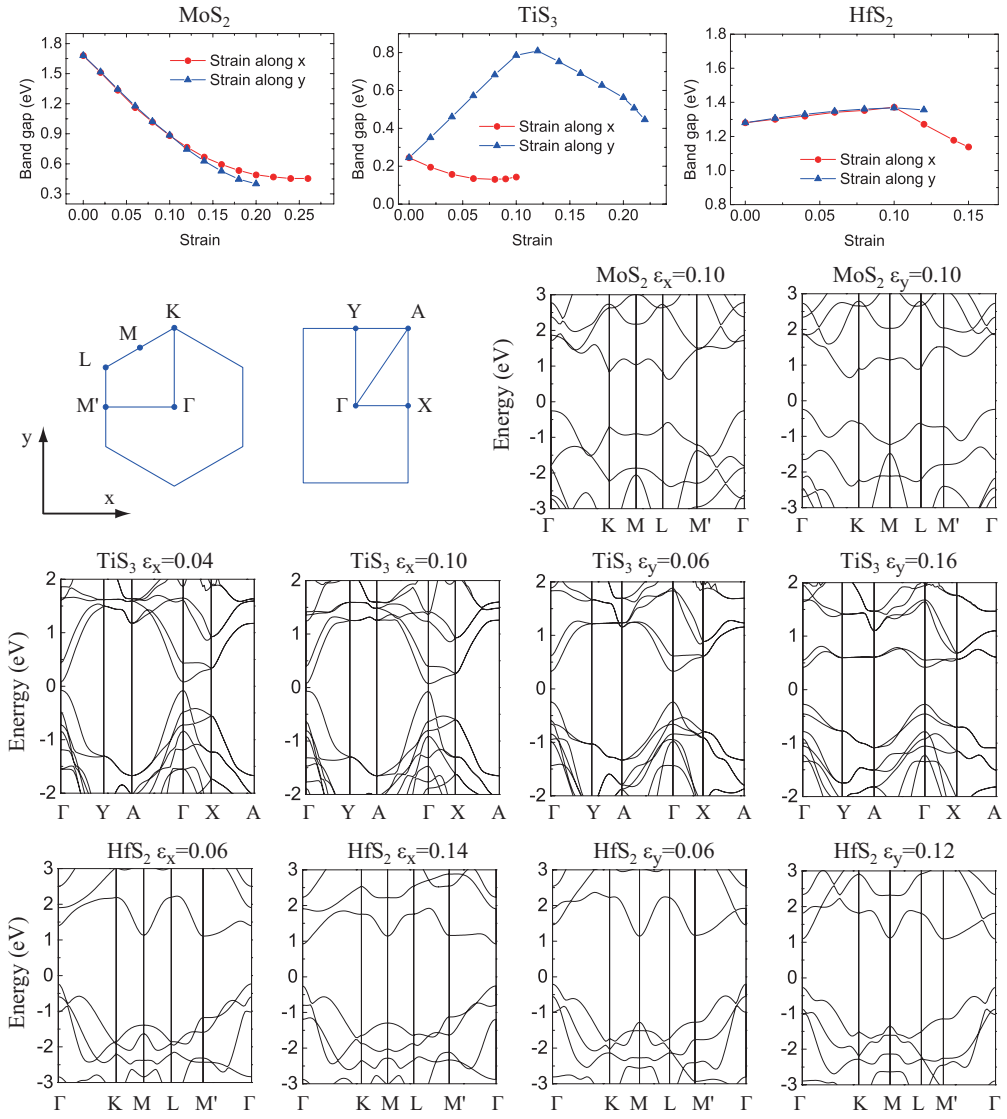

FIG. 2: The variation of band gap of MoS_2, TiS_3 and HfS_2 with strain, and the band structure under different strain. The corresponding Brillouin zones and high symmetry k-paths are also shown.

Kluwer Academic Publishers, Dordrecht, 1998, ISBN 0-7923-5255-6.

[3] W. A. Pryor, Inorganic Sulphur Chemistry. G. NICKLESS, Ed. Elsevier, New York, 1968.

[4] J. M. Hensen, V. H. J. De Beer, R. A. Van Santen Chemistry and Reactivity of Transition Metal Sulphides in Relation to Their Catalytic Performance, Transition Metal Sulphides, NATO ASI Series Volume 60, 1998, pp 169-188.

[5] J. Feng, X. Qian, C.-W. Huang and J. Li, Nature Photonics **6**, 866 (2012).

[6] X. Hong, J. Kim, S.-F. Shi, Y. Zhang, C. Jin, Y. Sun, S. Tongay, J. Wu, Y. Zhang and F. Wang, Nature Nanotechnology **9**, 682 (2014).

[7] M. Chhowalla, H. S. Shin, G. Eda, L.-J. Li, K. Ping Loh and H. Zhang, Nature Chemistry 5, 263 (2013).

[8] K. S. Novoselov, D. Jiang, F. Schedin, T. J. Booth, V. V. Khotkevich, S. V. Morozov, and A. K. Geim. PNAS 102 30 10451 (2005).

[9] Mak, K. F., Lee, C., Hone, J., Shan, J. and Heinz, T. F. Phys. Rev. Lett. 105, 136805 (2010).

[10] Bertolazzi, S., Brivio, J. and Kis, A. . ACS Nano 5, 9703 (2011).

[11] Matte, H. S. S. et al. Angew. Chem. Int. Ed. 49, 4059 (2010).

[12] Wang, Q. H., Kalantar-Zadeh, K., Kis, A., Coleman, J. N. and Strano, M. S., Nature Nanotech. 7, 699 (2012).

[13] C. Ataca, H. Sahin, and S. Ciraci, J. Chem. Phys. C **116**, 8983 (2012).

[14] Feng, J. et al. Adv. Mater. 24, 1969 (2012).

[15] C. Kreis, S. Werth, R. Adelung, L. Kipp, M. Skibowski, E. E. Krasovskii, and W. Schattke, Phys. Rev. B 68, 235331 (2003)

[16] J. O. Island, M. Buscema, M. Barawi, J. M. Clamagirand, J. R. Ares, C. Snchez, I. J. Ferrer, G. A. Steele, H. S. J. van der Zant and A. Castellanos-Gomez, Advanced Optical Materials 2, 7 641 (2014)

[17] M. Topsakal, S. Cahangirov, and S. Ciraci, Appl. Phys. Lett. **96**, 091912 (2010).
[18] S. Bertolazzi, J. Brivio, and A. Kis, ACS Nano **5**, 9703 (2011).
[19] J. Dai, and X. C. Zeng, arXiv:1501.02313 (2015).
[20] L. Brattas and A. Kjekshus, Acta Chem. Scand. **26**, 3441 (1972).
[21] J. Li, N. V. Medhekar, and V. B. Shenoy, J. Chem. Phys. C **117**, 15842 (2013).
[22] T. Li, Phys. Rev. B **90**, 167402 (2014)
[23] G. Kresse and J. Hafner, Phys. Rev. B **47**, 558 (1993).
[24] G. Kresse and J. Furthmller, Phys. Rev. B **54**, 11169 (1996).
[25] P. E. Blöchl, Phys. Rev. B **50**, 17953 (1994).
[26] J. P. Perdew, K. Burke, and M. Ernzerhof, Phys. Rev. Lett. **77**, 3865 (1996).
[27] H. J. Monkhorst and J. D. Pack, Phys. Rev. B **13**, 5188 (1976).